International Journal of Nanomedicine

Dovepress
Taylor & Francis Group

Open Access Full Text Article

ORIGINAL RESEARCH

Lung Epithelial Cell Membrane-Camouflaged ROS-Activatable Berberine Nanoparticles for Targeted Treatment in Acute Lung Injury

Chengkang Jin[1,*], Yingjie Zhang[2,*], Lin Chen[3,4,*], Bingqing Chen[5,*], Changjiang Chen[1], Hairui Zhang[1], Junping Guo[6,*], Wei Chen[7,*], Yi Shi[7], Chengping Wen[1]

[1]College of Basic Medical Science, Zhejiang Chinese Medical University, Hangzhou, 310053, People's Republic of China; [2]College of Pharmacy, Zhejiang University of Technology, Hangzhou, 310014, People's Republic of China; [3]School of Life sciences, Zhejiang Chinese Medical University, Hangzhou, 310053, People's Republic of China; [4]Biological Macromolecules Development Department, Hangzhou Zhongmeihuadong Pharmaceutical Co., Ltd, Hangzhou, 310011, People's Republic of China; [5]Yue Yang Hospital of Traditional Chinese & Western Medicine, Shanghai University of Traditional Chinese Medicine, Shanghai, 200437, People's Republic of China; [6]Rainbowfish Rehabilitation and Nursing School, Hangzhou Vocational & Technical College, Hangzhou, 310018, People's Republic of China; [7]Longhua Hospital Affiliated to Shanghai University of Traditional Chinese Medicine, Shanghai, 200032, People's Republic of China

*These authors contributed equally to this work

Correspondence: Chengping Wen, College of Basic Medical Science, Zhejiang Chinese Medical University, Hangzhou, 310053, People's Republic of China, Email wengcp@163.com; Yi Shi, Longhua Hospital Affiliated to Shanghai University of Traditional Chinese Medicine, 725 South WanPing Road, Shanghai, 200032, People's Republic of China, Tel +86 021 64385700 3522, Email lh2918@shutcm.edu.cn

Introduction: Acute lung injury (ALI) seriously threatens human health and is induced by multiple factors. When ALI occurs, lung lesions affect gas exchange and may trigger respiratory failure. Current clinical treatments are limited, and traditional drug delivery has drawbacks. Berberine, a natural drug with anti-inflammatory effects, has difficulty in effectively exerting its efficacy.

Methods: The study designed a nano-micelle. Hydrophobic berberine was encapsulated with diselenide bonds as the linker. Then, lung epithelial cell membranes were extracted to encapsulate and disguise the nano-micelle. These nanoparticles were injected intravenously. Thanks to the cell membrane's specificity, they could bind to lung tissue, achieving targeted lung delivery. In the inflamed area of acute lung injury, the significantly increased reactive oxygen species level was used to break the diselenide bonds, enabling precise berberine release at the lung injury site.

Results: The nano-drug (MM-NPs) was successfully prepared, with the encapsulation efficiency of berberine in the micelles reaching 68.2%. In a ROS environment, the nano-micelles could quickly release over 80% of berberine. In inflammatory MLE-12 cells, MM-NPs responded well to ROS, and cellular inflammatory factor levels were significantly improved after treatment. In a lipopolysaccharide (LPS)-induced pneumonia mouse model, MM-NPs achieved lung targeting. Further studies showed that MM-NPs administration significantly alleviated LPS-induced lung injury in mice. Additionally, evaluation indicated MM-NPs had good in-vivo safety with no obvious adverse reactions.

Conclusion: This study successfully developed a novel delivery system, MM-NPs, overcoming berberine's low bioavailability problem in treating acute lung injury. The system has excellent physicochemical properties, biocompatibility, and metabolic safety. In vitro and animal experiments verified it can significantly enhance the therapeutic effect, offering new ideas and hopes for acute lung injury treatment. In the future, clinical trials can be advanced, and new lung targeting strategies explored for more therapeutic breakthroughs.

Keywords: acute lung injury, berberine, nano-micelles, lung-targeted delivery, reactive oxygen species

Introduction

Acute lung injury is one of the major diseases that seriously threaten human health at present. Its onset is usually induced by a variety of complex factors, such as severe infection, major trauma and shock.[1,2] Once acute lung injury occurs, the lungs will quickly fall into a series of complex and extremely destructive pathological changes. A strong inflammatory

Received: 27 December 2024
Accepted: 7 May 2025
Published: 15 May 2025

reaction spreads in the lungs, and a large number of inflammatory factors are released,[3] leading to damage to lung tissue. The severe oxidative stress state exacerbates the degree of cell damage, making the lung cell function abnormal.[4] These pathological changes work together to seriously affect the gas exchange function of the lungs[5] and may even lead to respiratory failure, bringing great risks to the lives of patients.[6,7]

At present, the treatment methods for acute lung injury in clinical practice are relatively limited. Although mechanical ventilation support can maintain the respiratory function of patients to a certain extent, it cannot fundamentally solve the problem of lung injury.[8,9] Anti-infective treatment can only play a partial role in acute lung injury caused by infectious factors,[10] and the effect is not good for lung injury caused by other reasons. Therefore, there is an urgent need to develop more effective treatment strategies.

In the process of exploring new treatment methods, the natural medicine berberine gradually comes into people's view. Berberine, also known as berberine hydrochloride, widely exists in many natural plants.[11] In traditional medicine, berberine has been applied in the treatment of different diseases because of its various effects.[11] In recent years, with the deepening of scientific research, the rich pharmacological activities of berberine have been further revealed. It has a significant anti-inflammatory effect and can effectively inhibit the release of inflammatory factors[12,13] and reduce the inflammatory reaction in the lungs. In sepsis-related acute lung injury (ALI), berberine inhibits the excessive inflammatory response by regulating the ratio of regulatory T cells and T helper 17 cells.[14] In lipopolysaccharide (LPS)-induced ALI, berberine reduces the release of inflammatory factors such as interleukin-1β (IL-1β) by inhibiting the activation of the NLRP3 inflammasome,[15] and inhibits the overexpression of pro-inflammatory factors (such as tumor necrosis factor-α (TNF-α), interleukin-6 (IL-6), interleukin-8 (IL-8)) to alleviate the inflammatory response in lung tissues.[16] Berberine can also repair LPS-induced alveolar epithelial barrier damage by regulating the expression of tight junction proteins.[14] However, the traditional administration methods of berberine have many disadvantages. The oral bioavailability of berberine is extremely low, usually less than 1%.[17] Moreover, the concentration of berberine in plasma is low. It tends to accumulate in tissues such as the liver and intestines, while its distribution in the lungs is limited.[18] Therefore, due to its complex pharmacokinetic properties, berberine needs to be delivered via targeted delivery to break through the bottleneck in the treatment of acute pneumonia.

Multiple studies have confirmed that nanoparticles can reduce pulmonary edema and decrease the infiltration of inflammatory cells in animal models of acute lung injury (ALI). Bionic nanomedicines have demonstrated high translational potential in preclinical models.[19] Although biocompatible gold nanoclusters can alleviate ALI, their lung targeting ability needs to be enhanced. Lipid nanoparticles, as delivery carriers, can improve targeting and prolong the drug action time through optimized design.[20] Compared with liposomes and polymer nanoparticles, micelles have a higher drug loading capacity and better penetrability.[21] Therefore, we chose self-assembled micelles as the nanocarrier. Self-assembled micelles are spontaneously formed by amphiphilic block copolymers in aqueous solutions. The hydrophobic core can efficiently encapsulate poorly soluble drugs, while the hydrophilic shell provides colloidal stability. Using polyethylene glycol (PEG) as the hydrophilic end can prolong the blood circulation time;[22] choosing poly(lactic-co-glycolic acid) (PLGA) as the hydrophobic end, because it is a biodegradable material approved by the FDA and is widely used in human implants and drug carriers.[23] Its degradation products can be metabolized into carbon dioxide and water through the tricarboxylic acid cycle, without the risk of toxic accumulation.

There are mainly two problems. Firstly, there is the problem of targeting. The emergence of membrane-coated nanoparticles brings the possibility to solve the targeting problem.[24] At present, common membranes mainly come from natural cells such as red blood cells,[25] white blood cells,[26] platelets,[27] etc. This type of membrane camouflage relies on passive targeting: the enhanced permeability and retention (EPR) effect. Acute lung injury (ALI) can trigger the entrapment of nanoparticles by non-specific immune cells, resulting in a decrease in targeting efficiency.[28] Moreover, due to the special structure of pulmonary capillaries, it is difficult for passive targeting strategies to achieve efficient enrichment.[29] The surface of pulmonary epithelial cell membranes retains lung tissue-specific adhesion molecules such as Surfactant protein A (SP-A), which can achieve active targeting mediated by homologous membranes through the "homing to the same kind" mechanism. For example, some studies have used SP-A as a targeting receptor to deliver drugs to alveolar type II epithelial cells, indicating the potential application value of SP-A in lung tissue targeting.[30] There are also reports that lung-homing peptides achieve lung targeting by binding to C16-ceramide on the endothelial

cell membrane, suggesting that lipid molecules may be involved in the homing mechanism.[31] In conclusion, it is advisable to consider leveraging the targeting recognition ability of pulmonary epithelial cell membranes to achieve precise drug delivery.

Secondly, there is the issue of drug release. Drugs need to remain stable in the bloodstream and should be rapidly released once they reach the target site. Existing responsive releases mainly target pH response,[32] light response,[33] enzyme response,[34] etc., among which ROS responsiveness is the most common. Currently, most studies use disulfide bonds or thioester (TK) bonds. Disulfide bonds mainly rely on a high-concentration glutathione (GSH) environment or strong oxidation conditions for activation. However, their direct responsiveness to reactive oxygen species (ROS) is relatively weak. For example, disulfide bonds remain intact under 100 mm hydrogen peroxide (H_2O_2), while diselenide bonds break.[35] Moreover, their breaking speed is relatively slow, which may affect the timeliness of drug release.[36] Although the response specificity of TK bonds to ROS is better than that of disulfide bonds, their stability is weak. They break prematurely in the physiological environment, affecting the accuracy of drug delivery.[37] The diselenide bond has a selective response to reactive oxygen species.[38] Compared with other redox-active substances, the diselenide bond is more sensitive to reactive oxygen species and has a faster response speed.[39] The diselenide bond is used in the design and synthesis of drug delivery systems. Under normal physiological conditions, the drug delivery system can remain stable and prevent premature drug release.[40]

Based on this, we designed nano-micelles with diselenide bonds as connecting arms to encapsulate the hydrophobic drug berberine. At the same time, lung epithelial cell membranes were extracted for encapsulation and camouflage. After intravenous injection, this nanoparticle specifically binds to lung tissue with the help of cell membranes, thereby achieving efficient lung-targeted delivery. At the inflammatory site of acute lung injury, due to the significant increase in ROS levels,[41] the diselenide bond will break and berberine will be accurately released at the lung injury site. Berberine brings hope to damaged lung tissue by inhibiting the release of inflammatory factors and reducing oxidative stress damage in acute lung injury (Figure 1). However, the safety of long-term drug administration still needs to be taken into consideration in this study. For example, selenium has a tendency to accumulate in the liver and kidneys. In addition, exploring the universality of diselenide bonds in other low-reactive oxygen species (ROS) diseases will expand the clinical application scenarios of this platform. In short, this project brings new ideas for the treatment of ALI.

Materials and Methods

Materials

Selenocystamine dihydrochloride (NH2-(CH2)2-Se-Se-(CH2)2-NH2) (D303521), berberine (B414323), 1,5-pentanediamine hydrochloride (NH2-(CH2)5-NH2) (D111805), and cell membrane protein extraction kit (P0033) were obtained from Beyotime Biotechnology; Poly(lactic-co-glycolic acid) carboxylate (PLGA-COOH) (MW: 5000, LA:GA = 50:50) was obtained from Daigang Biotechnology Co., Ltd.; Dimethyl sulfoxide (DMSO), 1-ethyl-3-(3-dimethylaminopropyl) carbodiimide (EDC), and N-hydroxysuccinimide (NHS) were obtained from Shanghai Macklin Biochemical Co., Ltd.; Anti-Na+/K+-ATPaseα was purchased from Cell Signaling Technology (#3010); Pyrene and lipopolysaccharide from Escherichia coli 055:B5 (LPS) were obtained from Sigma-Aldrich (Shanghai) Trading Co., Ltd.; Methoxy polyethylene glycol carboxyl (m-PEG-COOH) (MW: 5000) was purchased from Shanghai Top-Bio Technology Co., Ltd.; 2',7'-Dichlorodihydrofluorescein diacetate (DCFH-DA) was purchased from MedChemExpress.

The Synthesis Routes of PLGA-(CH2)2-Se-Se-(CH2)2-PEG and PLGA-(CH2)5-PEG

PLGA-(CH2)2-Se-Se-(CH2)2-PEG is synthesized through a two-step amide reaction. Briefly, dissolve PLGA-COOH (100 mg), EDC (6 mg), and NHS (3.5 mg) in 10 mL of anhydrous DMSO. Then place it in a magnetic stirring water bath and activate it at 60 °C for 30 min. Then, NH2-(CH2)2-Se-Se-(CH2)2-NH2 (10 mg in anhydrous DMSO) is added and reacted for 24 hours. After that, dialysis is performed using a 3500 Da MWCO dialysis membrane. Subsequently, the intermediate product PLGA-(CH2)2-Se-Se-(CH2)2-NH2 is obtained by freeze-drying (FD-1A-5 vacuum freeze dryer). The intermediate product is further reacted with m-PEG-COOH through an amide reaction to generate PLGA-(CH2)2-Se-Se-(CH2)2-PEG. The amide reaction method is the same as described above. The difference is that before the

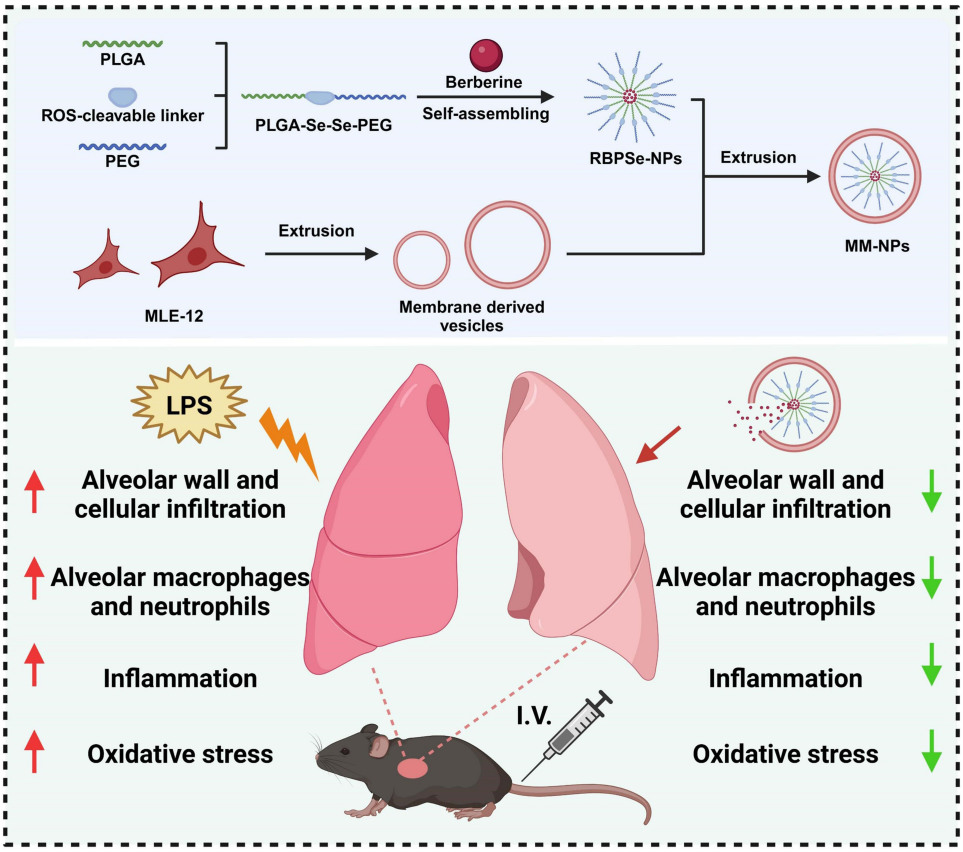

Figure 1 Schematic diagram describing the important role of MM-NPs in acute lung injury by inhibiting the release of inflammatory factors and reducing oxidative stress damage, and the design principle of how to construct a new delivery system (MM-NPs) in which ROS-responsive micelles carry berberine and wrap lung epithelial cell membranes.

dialysis operation, 90 mL of pure water is added and mixed thoroughly. Then, it is centrifuged at a speed of 12,000 rpm for 5 min to remove the precipitate.

PLGA-(CH2)5-PEG is also generated through a two-step amide reaction. In this case, NH2-(CH2)2-Se-Se-(CH2)2-NH2 is replaced by NH2-(CH2)5-NH2.

The above polymer was confirmed by 1H NMR in DMSO-d6 (Nuclear Magnetic Resonance Spectrometer AC-80). And PLGA-(CH2)2-Se-Se-(CH2)2-NH2 was further corroborated through FTIR analysis (Infrared spectrometer BRUKER ALPHA II).

CMC Measurement

The critical micelle concentration (CMC) of PLGA-(CH2)2-Se-Se-(CH2)2-PEG and PLGA-(CH2)5-PEG was determined by the pyrene fluorescence probe method. 10 mg of the PLGA-(CH2)2-Se-Se-(CH2)2-PEG or PLGA-(CH2)5-PEG was dispersed in 10 mL of distilled water, and then probe sonication was performed 20 times at a power of 400 W for 2 seconds with a pause of 3 seconds to prepare a 1 mg/mL aqueous solution of the graft (Ultrasonic cell disruptor SCIENTZ-IID). The solution was then diluted to a concentration range of 0.005 to 1 mg/mL. Next, a certain amount of pyrene was added to each solution to make the final concentration of pyrene reach 6×10^-7 mol/L. After ultrasonic treatment in a water bath for 30 minutes, the emission spectrum of pyrene was recorded using a fluorescence spectrophotometer with an excitation wavelength of 337 nm. The fluorescence intensities at emission wavelengths of 373 nm and 384 nm were recorded. The CMC of the two micelles was calculated using the I373/I384 ratio. The CMC was obtained by piecewise linear regression. The experimental data were divided into low-concentration and high-concentration regions, and the data in the two regions were fitted with straight lines respectively. The intersection point of the two straight lines was calculated, and the corresponding concentration was the CMC.

Steps for Extracting Cell Membranes

Steps for extracting cell membranes.[42] Cultivate about 20 to 50 million cells. Wash once with PBS. Treat the cells with a cell digestion solution containing EDTA but without trypsin to make the cells no longer adhere very tightly. Use a pipette to blow down the cells. Centrifuge to collect the cells, aspirate the supernatant, and leave the cell pellet for later use. Try to avoid digesting cells with trypsin as much as possible to prevent trypsin from degrading membrane proteins. Then extract the cell membrane according to the cell membrane protein extraction kit (P0033) from Beyotime Biotechnology. The mouse alveolar epithelial cells MLE-12 were purchased from Wuhan Procell Life Science & Technology Co., Ltd.

Preparation of RBPSe-NPs, BPC-NPs, MM-NPs and MMC-NPs

ROS-responsive berberine nano-micelles (RBPSe-NPs) were prepared by dropwise dialysis method.[38] PLGA-(CH2) 2-Se-Se-(CH2)2-PEG with a concentration of 10 mg/mL and berberine solution with a concentration of 2.5 mg/mL were prepared with methanol as solvent. 1 mL of PLGA-(CH2)2-Se-Se-(CH2)2-PEG solution and 400 μL of berberine solution were mixed and slowly dropped into double distilled water. At the same time, it was heated to 60 degrees Celsius and stirred for 1 h. Subsequently, dialysis was performed for 24 h with a dialysis membrane of 3500 daltons, and the water was changed intermittently. Then, RBPSe-NPs were obtained by freeze-drying.

A solution of RBPSe-NPs and MLE-12 cell membrane with the same concentration was prepared. The cell membrane was wrapped outside RBPSe-NPs by using a liposome extruder to obtain membrane-mimicking ROS-responsive berberine nano-micelles (MM-NPs).

PLGA-$(CH_2)_5$-PEG is used as a carrier to encapsulate berberine by dropwise dialysis method to obtain non-ROS-responsive control berberine nano-micelles (BPC-NPs). Prepare solutions of BPC-NPs and MLE-12 cell membranes with the same concentration. Use a liposome extruder to wrap the cell membrane outside BPC-NPs to obtain membrane-mimicking berberine nano-micelles (MMC-NPs).

The Concentration Calibration Curve of Berberine

Precisely weigh 5 mg of berberine and add it to 20 mL of phosphate buffered saline (PBS). Use a 60°C water bath to assist dissolution and prepare a stock solution with a concentration of 0.25 mg/mL. Then dilute it to the required concentration with PBS.

The absorbance spectrum of berberine was detected by a spectrophotometer, and the maximum absorption wavelength of berberine (346 nm) was obtained. Berberine solutions with concentrations of 40, 35, 30, 25, 20, 15, 10, 5, and 0 μg/mL were prepared respectively, and their absorbance intensities at 346 nm were detected. The standard curve regarding berberine concentration was calculated according to the absorbance intensity.

Characterization of Nanoparticles

Weigh precisely 10 mg of each nanoparticle, disperse it in 10 mL of deionized water, perform probe sonication 20 times at a power of 400 W, with a working time of 2 s and a pause time of 3 s to prepare an aqueous nanoparticle solution with a concentration of 1 mg/mL. Subsequently, the size distribution and zeta potential data were measured via dynamic light scattering (DLS; Litesizer 500, Anton-Paar, Austria); The morphology was observed by transmission electron microscopy (TEM; JEM-1400flash, JEOL, Japan). The ultraviolet-visible spectrum and fluorescence spectrum of synthesized nanoparticles were obtained on a UV-visible absorption spectrophotometer (UV-2600, SHIMADZU, Japan) and a fluorescence spectrophotometer (FP 6500, JASCO, Japan), respectively.

To evaluate the physical stability of the nano-micelles, an aqueous solution of nano-micelles with a concentration of 1 mg/mL was taken. The micelle solution was aliquoted into 7 groups of sample vials (with at least 3 parallel samples in each group and 1 mL in each vial), labeled as T0, T2, T4, T6, T8, T10, and T12, corresponding to the detection time points of 0 day, 2 days, 4 days, 6 days, 8 days, 10 days, and 12 days, respectively. The aliquoted sample vials were placed in a constant-temperature incubator at 37 °C and stored in the dark. The T0 group was immediately tested, and the remaining groups were stored for the corresponding time and the particle size was measured at the corresponding time.

In order to calculate the production rate and encapsulation efficiency of micelles, the dialysate generated during the preparation of RBPSe-NPs was collected. The intensity of ultraviolet absorption light at 346 nm was measured. The concentration was calculated according to the standard curve of berberine concentration. The mass of berberine not incorporated into the micelles was calculated based on the volume and concentration of the dialysate. The production rate (PB) of RBPSe-NPs, that is, the content of berberine encapsulated in the total micelles, was calculated using Eq. 1:

$$\mathrm{PB} = \frac{\text{weight of berberine in micelles}}{\text{weight of feeding berberine} + \text{weight of feeding materials}} \times 100\,\%$$

The encapsulation efficiency (EB) of berberine during the micelle encapsulation process was calculated using Eq. 2:

$$\mathrm{EB} = \frac{\text{weight of berberine in micelles}}{\text{weight of feeding berberine}} \times 100\,\%$$

In vitro Drug Release

The release curve of berberine in RBPSe-NPs was determined by dialysis method. Each sealed dialysis bag (with a molecular weight cut-off of 3500 Da) containing 1 mL of RBPSe-NPs with 500 μg of berberine was immersed in 40 mL of phosphate buffered saline solution containing 1 mm hydrogen peroxide (H_2O_2) and phosphate buffered saline solution only containing phosphate buffered saline solution (pH 7.4). Subsequently, they were all placed in a constant temperature incubator at 37 °C. Dialysate was collected at 0.25, 0.5, 1, 2, 4, 8, 12, 20, 24, 36, 48, and 50 hours, and the same volume of fresh dialysate was replenished. A spectrophotometer was used to measure all the collected dialysate to determine the cumulative release of berberine from RBPSe-NPs.

SDS-PAGE Assay

The membrane protein of MM-NPs was determined by sodium dodecyl sulfate-polyacrylamide gel electrophoresis (SDS-PAGE). For the analysis, MLE-12 cells, MLE-12 cell membranes, MMC-NPs, and MM-NPs were first lysed with RIPA lysis buffer containing protease inhibitor cocktail on ice for 20 minutes. Thereafter, the lysates were centrifuged at 13500 rpm for 5 minutes at 4 °C. Then, the supernatant was measured by the BCA Assay Kit (Beyotime, Shanghai, China) to quantify the total protein. An equal amount of 30 micrograms of protein per sample was mixed with SDS-PAGE loading buffer and heated at 100 °C for 5 minutes. Samples were loaded equally into the wells of 10% SDS-PAGE gel for electrophoresis analysis in an electrophoresis chamber system. Protein was stained with Coomassie blue fast staining solution (Beyotime, Shanghai, China) and washed three times with destainer (water/methanol/acetic acid, 9:9:2) for 5 minutes each.

Western Blot Assay

After lysing cells with RIPA (Beyotime, Shanghai, China) to obtain protein samples, the protein concentration was measured by the BCA method. After electrophoresis, 5% skimmed milk was used for blocking at room temperature for 2 hours. The primary antibody was incubated overnight at 4°C, and the secondary antibody was incubated for 1 hour at room temperature. Anti-Na+/K+-ATPase α was obtained from Cell Signalling Technology (1:1000 dilution)(#3010). The peroxidase-conjugated secondary antibody (1:4000 dilution) was used, and ECL reagent (Beyotime, Shanghai, China) was added at a 1:1 ratio to develop the image on a digital imaging system (Bio-Rad, USA).

LPS Induced Cell Inflammation

1×10^5 MLE-12 cells were cultured in a six-well plate. After the cells adhered, the culture medium was replaced with a medium containing 1 μg/mL LPS and cultured for 1 day.

Reactive Oxygen Species Detection

Cells were incubated in a medium containing DCFH-DA (20 μM) in a 6-well plate for 30 minutes. Then, the cells were collected, fixed, and counterstained with DAPI. The DCF fluorescence intensity was immediately detected using confocal laser scanning microscopy (CLSM) and quantitatively analyzed using ImageJ software (National Institutes of Health).

For each sample, 1×105 cells were stained with DCFDA in a 37°C, 5% CO2 incubator for 30 minutes. After filtration, the samples were loaded onto a flow cytometer for detection and quantification.

Cell Uptake of Nanomedicines

LPS-induced inflammatory MLE-12 cells (1×10^5 cells per well) were treated with MM-NPs at concentrations of 2, 4, 8, 16, and 32 μg/mL (according to the content of berberine) for 4 hours. Subsequently, the cell membrane was labeled with the membrane dye DID and then fixed with 4% paraformaldehyde. Laser confocal scanning microscopy (laserA1R, Nikon, Japan) imaging was used to characterize the distribution of nanoparticles.

Inflammatory MLE-12 cells (1×10^5 cells per well) were treated with MM-NPs (16 μg/mL of berberine content) for 4 hours and 8 hours. Subsequently, the cell membrane was labeled with the membrane dye DID and then fixed with 4% paraformaldehyde. Laser confocal scanning microscopy (laserA1R, Nikon, Japan) imaging was used to characterize the distribution of nanoparticles.

Inflammatory MLE-12 cells (1×10^5 cells per well) were treated with free berberine, RBPSe-NPs, MMC-NPs, and MM-NPs (16 μg/mL of berberine content) for 4 hours; normal MLE-12 cells (1×10^5 cells per well) were treated with RBPSe-NPs and MM-NPs (16 μg/mL of berberine content) for 4 hours. Subsequently, the cell membrane was labeled with the membrane dye DID and then fixed with 4% paraformaldehyde. Laser confocal scanning microscopy (laserA1R, Nikon, Japan) imaging was used to characterize the distribution of nanoparticles.

Colocalization of Nanomedicines and Mitochondria

MLE-12 cells were incubated with MM-NPs for 4 hours. Then, an appropriate amount of Mito-red dye diluted with cell culture medium was added to ensure that the dye could fully cover the cells. After incubation for 30 minutes in a 37°C cell incubator. Fluorescence excitation was imaged by confocal laser scanning microscopy (CLSM), and co-localization was analyzed using ImageJ software (NIH).

Quantitative Real-Time PCR (qRT-PCR)

Total RNA was extracted from cell pellets or flash-frozen lung tissues using Trizol reagent (Thermo, USA). Reverse transcription of RNA samples was performed using a reverse transcription kit (gDNA wiper, Vazyme, R22201). The resulting cDNA samples were diluted 5–10 times with DEPC-treated water and stored at −20°C. Subsequently, real-time quantitative PCR (qRT-PCR) was conducted using SYBR Green Master Mix (Accurate Biology, AG11701) on an ABI Prism 7500 sequence detection system (Applied Biosystems, USA). The qRT-PCR data were normalized to β-actin, and the fold changes of target mRNAs were analyzed using the 2−ΔΔCT method. The primer sequences are shown in Table S1.

Mice

C57BL/6 (C57) mice were obtained from Hangzhou Medical College and maintained under specific pathogen-free (SPF) conditions, with a 12-hour light/12-hour dark cycle and free access to food and water. All animal experiments were approved by the Scientific Investigation Committee of Zhejiang Laboratory Animal Center (ZJCLA-IACUC-20011006). And comply with "General Principles of Laboratory Animal Welfare, GB/T 42011–2022".

Fluorescence Imaging in Mice

Acute lung injury mice were administered DID-stained MM-NPs and MMC-NPs, as well as RBPSe-NPs synthesized by replacing berberine with DID. Imaging was performed using an in vivo fluorescence imaging system (Perkin Elmer IVIS Spectrum CT Imaging System) at 3, 6, 12, 24, 48, and 72 hours after injection. The excitation wavelength is 535 nm and the emission range is 640–660 nm. After that, the mice were sacrificed and their major organs (heart, liver, spleen, lungs, and kidneys) were collected for ex vivo imaging.

Animal Experiment

In in vivo experiments, lipopolysaccharide (O55:B5, Sigma, USA) was instilled intratracheally into 8-week-old C57BL/6 mice at a dose of 4 mg/kg body weight to establish an acute lung injury model. Four hours later, the mice were treated by

tail vein injection of MM-NPs (berberine: 2 mg/kg), etc. There were 5 mice in each group. Twenty-four hours later, the mice were sacrificed for subsequent experiments.

Collected bronchoalveolar lavage fluid. Centrifuged it at 1300 rpm for 5 minutes at 4 °C to remove cells and impurities. Took the supernatant and measured the protein concentration using the BCA method. The increase in protein concentration was a marker of the disruption of the alveolar-capillary barrier.

Collected the lungs, fixed and dehydrated them, and then embedded them in paraffin. Subsequently, hematoxylin and eosin (H&E) staining was performed for histological examination. Scoring criteria: 0: Normal alveolar structure; 1: Mild interstitial thickening; 2: Thickening of the alveolar wall with a small amount of inflammatory cell infiltration; 3: Destruction of the alveolar structure with extensive inflammatory cell infiltration; 4: Severe pulmonary consolidation or hemorrhage.

Flow Cytometry of BALF Cells

Bronchoalveolar lavage fluid was collected and centrifuged at 1300 rpm for 5 minutes at 4 °C. The cells were resuspended in PBS for precipitation. The total number of cells in the bronchoalveolar lavage fluid of each mouse was counted under a microscope. The corresponding doses of flow cytometry antibodies for monocyte-derived macrophages (anti-CD45+, anti-F4/80+, anti-CD11b+) and neutrophils (anti-CD45+, anti-CD11b+, anti-Ly6G+) were successively added to each centrifuge tube. After thoroughly mixing the antibody with the cell suspension, the cells were incubated in the dark at 4 °C for 30 minutes and then detected by flow cytometry (BD Biosciences). Subsequently, FlowJo v10.8.1 was used for data analysis. The gating strategy of macrophages for flow cytometry is shown in Figure S1, and the gating strategy of neutrophils for flow cytometry is shown in Figure S2.

RNA Sequencing

Lung tissues from the pneumonia model control group and the MM-NPs treatment group were obtained. RNA sequencing and raw data quality control were performed by Shanghai Majorbio Biomedical Technology Co., Ltd. The data were analyzed on the online platform of Majorbio Cloud Platform. Genes with $|\log2 \text{(fold change)}| \geq 1$ and $p \leq 0.05$ were identified as differentially expressed genes.The gene sets of mouse molecular signatures were obtained through msigdbr (version 7.0.1, https://cran.rproject.org/web/packages/msigdbr/index.html). In this package, the original human genes of the Molecular Signatures Database (MSigDB v7.0, http://software.broadinstitute.org/gsea/msigdb/index.jsp) were converted to non-human model organism homologous genes.

Histopathological Examination and Blood Biochemistry Test

Routinely, the major organs were collected, fix them, dehydrate, and embed in paraffin, followed by H&E (hematoxylin and eosin) staining for histological examination.

For the complete blood count (CBC), 100 μL of fresh blood from each mouse was collect in EDTA solution, and counts with a Celltac Alpha MEK-6400 series hematology analyzer (Nihon Kohden, MEK-6400). For serum biochemical analysis, collect blood samples were coagulate at room temperature for 2 hours or overnight at 4°C, followed by centrifugation at 1000× g for 10 minutes to obtain the serum. Aliquot 150 μL of serum was then subjected to analysis for alanine aminotransferase (ALT), aspartate aminotransferase (AST) and creatinine (CR) using a chemistry analyzer (Mindray, BS-350E).

Statistical Analysis

All data analysis was performed using GraphPad Prism 8.0. Data were presented as mean ± standard error (SE) (n = 3 unless otherwise stated). The significance of the data was evaluated according to unpaired two-sided Student's *t*-test. When performing an independent samples *t*-test, the homogeneity of variance test is first carried out. If the variances are homogeneous, a *t*-test assuming equal variances is used; if the variances are heterogeneous, a *t*-test assuming unequal variances is used. For comparisons among three or more groups, one-way ANOVA was performed, and Tukey's test was used for multiple comparisons. *P < 0.05, **P < 0.01, ***P < 0.001, ****P < 0.0001, NS: not significant.

Results and Discussion

Preparation and Characterization of Nanomedicines

To promote the preferential accumulation of berberine in ALI-infected cells, we intended to develop targeted nanotherapies. Since high reactive oxygen species is a typical characteristic of the inflammatory microenvironment, reactive oxygen species-responsive drug delivery systems may be a potential approach to improve the efficacy of ALI.

Reactive oxygen species-responsive nanoparticles were prepared by self-assembly of the amphiphilic oxidation-sensitive micelle PLGA-(CH2)2-Se-Se-(CH2)2-PEG (PLGA-Se-Se-PEG). PLGA-Se-Se-PEG was obtained through two successive amide reactions. Its structure was verified by 1H NMR spectroscopy (Figure S3). The chemical shift of selenocystamine dihydrochloride appears at ≈0.75–1.5 ppm, which is the proton peak of the methylene group on selenocystamine dihydrochloride. When performing infrared spectroscopy analysis on the synthesized product PLGA-$(CH_2)_2$-Se-Se-$(CH_2)_2$-PEG, a series of characteristic absorption peaks were observed (Figure S4). The appearance of these peaks strongly demonstrated the successful synthesis of the target product. In the infrared spectrum of m-PEG-COOH, a strong and sharp absorption peak appeared at around 1715 cm^{-1}. This peak was attributed to the stretching vibration of the carboxyl C=O. For PLGA-COOH, relevant characteristic peaks were as follows: in the infrared spectrum of PLGA-COOH, a C=O stretching vibration peak appeared at around 1730 cm^{-1}, corresponding to the characteristic absorption of the ester carbonyl in the polyester segment. In the infrared spectrum of the final synthesized product, the peak at this position still existed and showed a trend of superposition and enhancement. In addition, a set of peaks in the range of 2850–2950 cm^{-1} were attributed to the C-H stretching vibration of the alkyl chain in the PLGA molecule, further confirming the presence of PLGA. For the raw material NH_2-$(CH_2)_2$-Se-Se-$(CH_2)_2$-NH_2, a relatively weak absorption peak appeared in the range of 850–950 cm^{-1}, corresponding to the stretching vibration of the Se-Se bond, proving that the structure containing the diselenide bond was retained in the final product. In aqueous solution, one end of the poly(lactic-co-glycolic acid) of PLGA-Se-Se-PEG acts as a hydrophobic side chain, which will aggregate to form a hydrophobic core. The hydrophilic main chain of PLGA-Se-Se-PEG will spread outward around the hydrophobic core to form RPSe-NPs with a micelle structure, and its micelle concentration is 7 μg/mL (Figure S5). Subsequently, as shown in Figure 2A, nanoparticles loaded with hydrophobic Berberine (RBPSe-NPs) were obtained through a simple self-assembly process. The production rate (PB) of RBPSe-NPs was 6.2%, and the encapsulation efficiency (EB) of berberine in micelles was 68.2%. Transmission electron microscopy (TEM) analysis showed that these nanoparticles had a uniform spherical morphology (Figure 2B). The micelles can remain stable for 2 weeks at 37 °C (Figure 2C). It is well known that when there is reactive oxygen species in the environment, the diselenium bond can be oxidized and broken, and it is sensitive to reactive oxygen species, especially hydrogen peroxide. The reaction process involves the oxidation of selenium atoms. After the diselenium bond is converted into selenium oxide, the bond breaks. Therefore, in the presence of H_2O_2 (overproduced in inflammatory tissues), PLGA-Se-Se-PEG will be degraded. To confirm the ROS responsiveness, we used 10 mm H_2O_2 to simulate the oxidative environment (high ROS) in ALI tissues, while PBS was similar to normal tissue conditions. According to the calculation of the standard curve of berberine content (Figure S6), among them, RBPSe-NPs rapidly accumulated and released more than 80% of berberine in a high ROS environment because the diselenium bond in the structure of RBPSe-NPs is sensitive to ROS (Figure 2D). The cleavage of the diselenide bond dominates the release process. The rapid release at the initial stage can quickly reach the effective drug concentration to inhibit the acute inflammatory storm. The slow release in the later stage prolongs the local drug retention time to counteract the persistent oxidative stress. Secondly, the ROS-responsive release achieves chemical targeting, confining the drug to the lesion area, improving the local drug bioavailability, and reducing the systemic toxicity.

To synthesize MM-NPs, the surface of ROS-responsive NPs was coated with cell membranes derived from the mouse lung epithelial cell line (MLE-12 cells) by extrusion method (Figure 2E). MM-NPs showed a spherical core-shell structure under TEM, and each nanoparticle was wrapped by a single layer of cell membrane (Figure 2F). Dynamic laser scattering (DLS) indicated the change in zeta potential of nanoparticles after drug loading and cell membrane encapsulation, and the zeta potential of MM-NPs was more negative than that of RBPSe-NPs (Figure 2G), which was consistent with the zeta potential on the surface of lung epithelial cells. In addition, DLS analysis showed the change in particle size of nanoparticles after drug loading and cell membrane encapsulation. After cell membrane coating, the diameter of

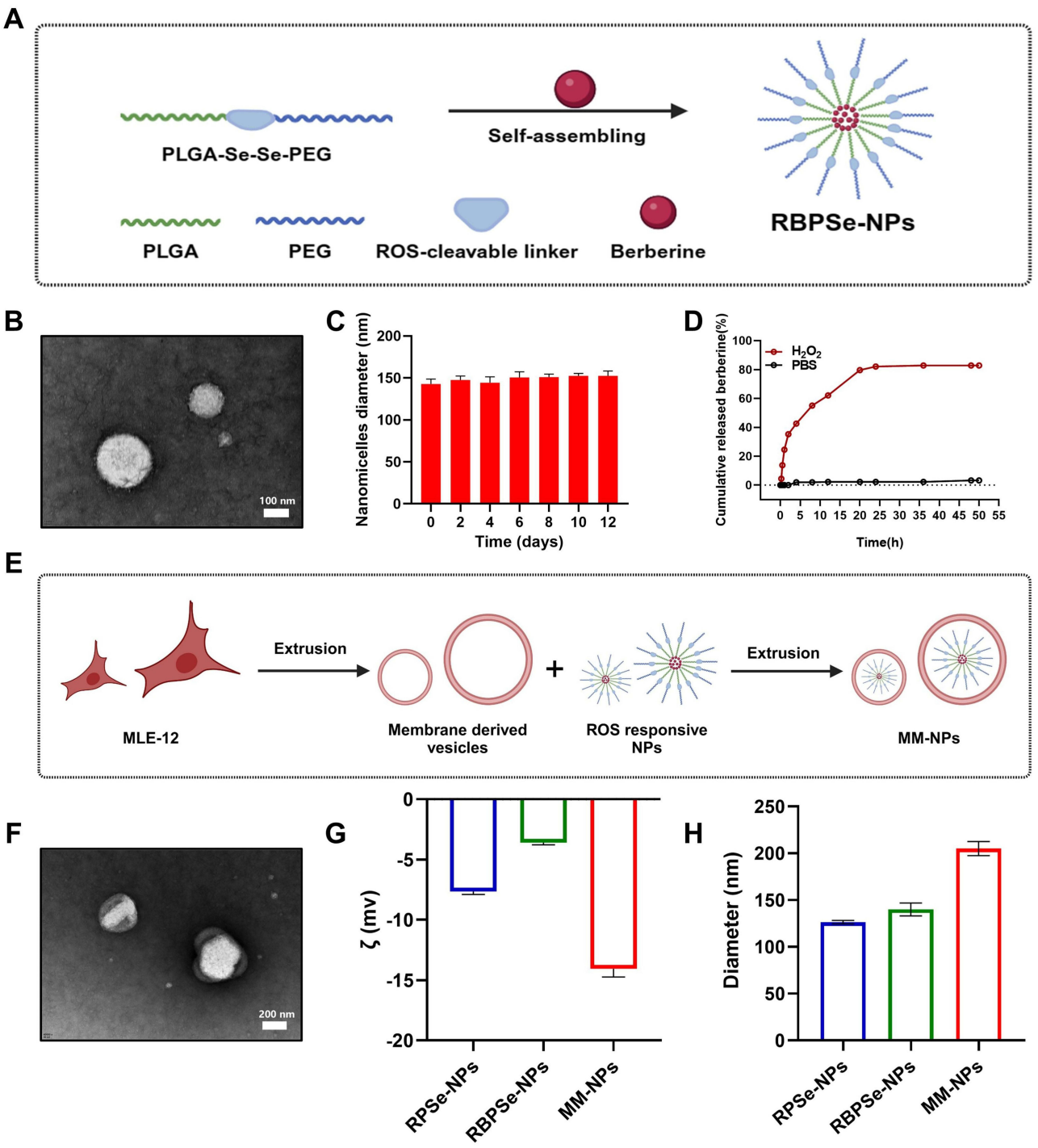

Figure 2 Preparation and characterization of nanomedicines. (**A**) Schematic illustration of the preparation of RBPSe-NPs. (**B**) TEM images of RBPSe-NPs. Scale bar = 100 nm. (**C**) RBPSe-NPs could maintain stability at 37 °C for 2 weeks. (**D**) RBPSe micelles can rapidly accumulate and release more than 80% of berberine because the diselenide bond in the structure of RBPSe is sensitive to reactive oxygen species. (**E**) Schematic illustration of preparation of MM-NPs through an extrusion method. (**F**) TEM images of MM-NPs. Scale bar = 200 nm. (**G**) Zeta potentials of NPs analyzed by DLS. (**H**) Particle sizes of NPs analyzed by DLS.

nanoparticles was about 150 to 200 nm (Figure 2H), which was again consistent with the addition of the lung epithelial cell membrane bilayer. In addition, Coomassie brilliant blue method and Western blot analysis confirmed that the lung epithelial cell membrane was successfully wrapped on the ROS-responsive nanoparticles (Figure S7). Although the synthesis of MM-NPs involves the integration of multiple steps, the core materials and processes have a basis for scalability. As a biomaterial approved by the FDA, PLGA has mature large-scale synthesis and purification processes.

The amide reaction between the amino group of the diselenide bond and the carboxyl group of PLGA occurs under mild conditions, avoiding the need for high temperature or high pressure, and is compatible with the conventional GMP environmental conditions. However, regarding the extraction of lung epithelial cell membranes, the ultracentrifugation method for separating cell membranes is feasible on a laboratory scale. But when scaled up, continuous-flow centrifugation or membrane filtration technologies are required to increase the throughput.

As a control, PLGA-(CH2)5-PEG was synthesized, and its structure was verified by 1H-NMR spectroscopy (Figure S8). The chemical shift of 1,5-pentanediamine hydrochloride appears at ≈0.75–1.5 ppm, which is the proton peak of the methylene group on 1,5-pentanediamine hydrochloride. PLGA-(CH2)5-PEG lacks sensitivity to the oxidative environment compared to PLGA-Se-Se-PEG, but still has micelle properties. Nanoparticles loaded with hydrophobic Berberine (BPC-NPs) are formed by self-assembly, and its micelle concentration is 6 μg/mL (Figure S9). We also verified the stability of BPC-NPs and their insensitivity to ROS (Figure S10A and S10B). And also analyzed the changes of zeta potential and particle size after drug loading and coating lung epithelial cell membranes by DLS (Figure S10C and S10D).

ROS Response of MM-NPs in Inflammatory MLE-12 Cells and Improvement of Inflammatory Factors

High reactive oxygen species is a typical characteristic of the inflammatory microenvironment. To explore whether it can be used for specific drug delivery, we compared the ROS levels of normal MLE-12 cells and LPS-induced MLE-12 cells. LPS-induced cell inflammation is a widely recognized method for studying the mechanism of inflammatory responses.[43] 2',7'-dichlorofluorescein diacetate (DCFH) is a commonly used fluorescent probe for detecting intracellular reactive oxygen species (ROS) levels. Observed by confocal laser scanning microscopy (CLSM), the DCFH probe produced green fluorescence in LPS-treated MLE-12 cells (Figure 3A). And normal MLE-12 cells and LPS-induced MLE-12 cells with added DCFH probes were collected and detected by flow cytometry (Figure 3B). The statistical ratio of the ROS content of the two is significantly different (Figure 3C). This result clearly confirms that LPS-induced MLE-12 cells produce a high reactive oxygen species environment, providing an important basis for subsequent studies on the role of high reactive oxygen species in the inflammatory microenvironment and the feasibility of specific drug delivery.

1,1'-Octadecyl-3,3,3',3'-tetramethylindodicarbocyanine perchlorate (DID) is a lipophilic fluorescent dye that can be used to label cell membranes and emit red fluorescence after binding to cell membranes. Berberine has certain fluorescent properties and can emit green fluorescence. We used CLSM to observe the intracellular uptake of the prepared MM-NPs in LPS-induced MLE-12 cells. We found that the uptake efficiency of nanoparticles increased with concentration and was the highest when the berberine concentration reached 16 μg/mL (Figure S11). And the uptake of nanoparticles also shows time dependence (Figure S12). In addition, as shown in Figure 3D and its fluorescence quantitative statistical results (Figure 3E), the green fluorescence of the MM-NPs group and the RBPSe-NPs group in LPS-induced MLE-12 cells is stronger than that of normal MLE-12 cells, and in LPS-induced MLE-12 cells, the green fluorescence of the MM-NPs group is stronger than that of the free Berberine group, the RBPSe-NPs group and the MMC-NPs group. The strong green fluorescence in the MM-NPs group in LPS-induced MLE-12 cells proves the response and release of the nanoparticles to the high ROS environment, which is of great significance for the targeted treatment of inflammatory diseases. The high ROS environment is usually related to inflammation. Nanoparticles can release drugs in this environment, and it is expected to achieve precise treatment. Coating the lung epithelial cell membrane increases the uptake efficiency of cells for materials. This finding provides a new strategy for improving the targeting and effectiveness of drug delivery.

Next, since mitochondria play a key role in inflammation and their oxidation level is manifested as an increase in inflammation, we studied whether the delivery of MM-NPs targets mitochondria. The mitochondrial red fluorescent probe (Mito-Tracker Red CMXRos) is a cell-permeable X-rosamine derivative that can specifically label biologically active mitochondria in cells and detect mitochondrial membrane potential. Red fluorescence representing mitochondria was observed in the cytoplasm by CLSM (Figure 3F). For the green fluorescence obtained by MM-NPs from the Berberine channel, it significantly overlaps with the red fluorescence, producing an obvious yellow color. And the fluorescence pixel overlap of MM-NPs is analyzed by Image J (Figure 3G). This proves the colocalization of ROS-

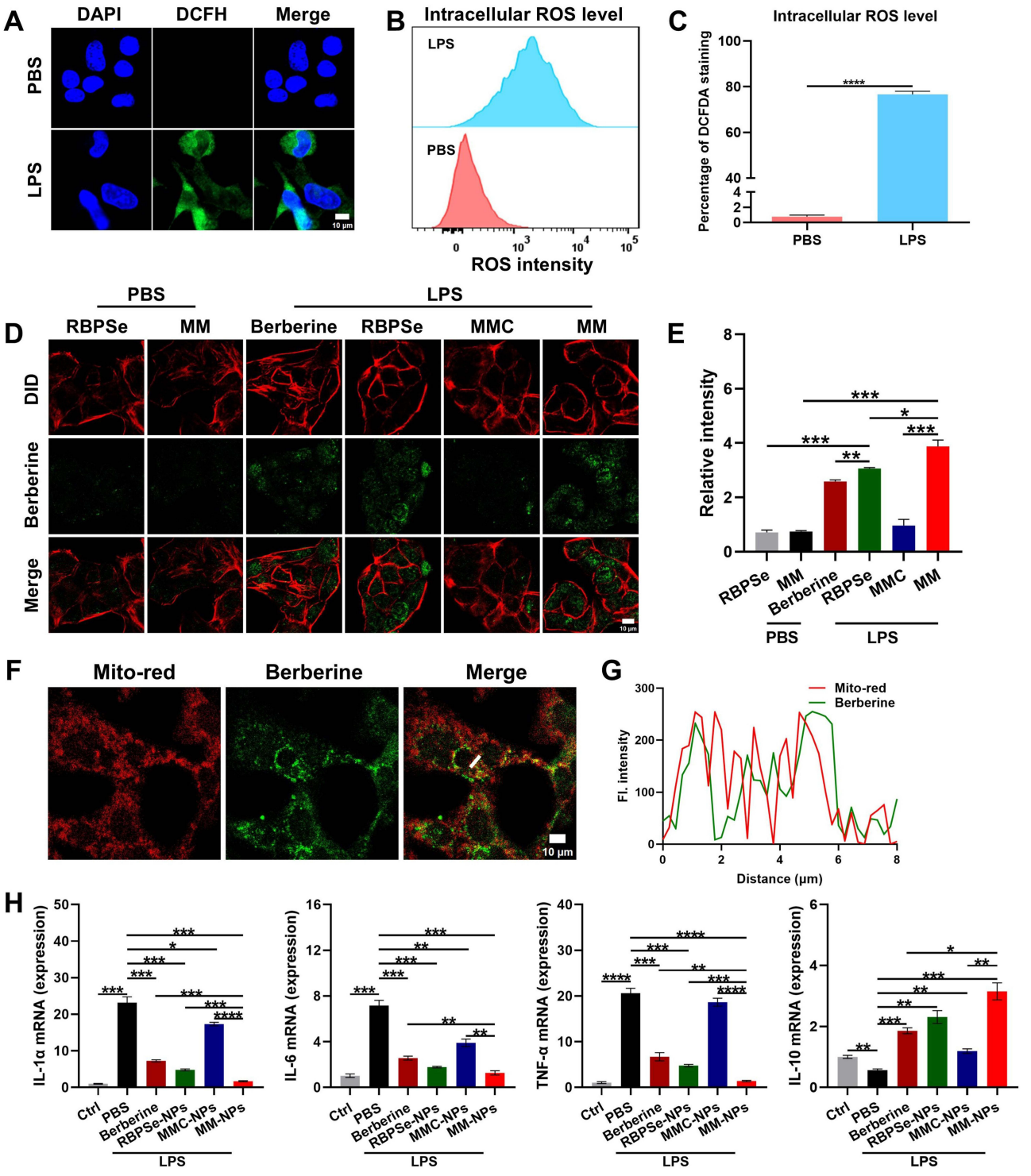

Figure 3 ROS response of MM-NPs in inflammatory MLE-12 cells and improvement of inflammatory factors. (**A**) Confocal images on detecting and comparing the levels of reactive oxygen species in LPS-induced inflammatory and normal lung epithelial cells. DCFH (green, a probe for detecting ROS), DAPI (blue, a nuclear stain). Scale bar, 10 μm. (**B**) Flow cytometry plots on detecting and comparing the levels of reactive oxygen species in LPS-induced inflammatory and normal lung epithelial cells. (**C**) Quantitative statistics of flow cytometry results in (**B**). (**D**) Detect the uptake of MM-NPs in lipopolysaccharide (LPS)-induced inflammatory lung epithelial cells and normal lung epithelial cells through confocal images, and detect the uptake efficiency of MM-NPs compared with free berberine, RBPSe-NPs and MMC-NPs. Scale bar, 10 μm. (**E**) Perform fluorescence quantification of the uptake in parallel images in (**D**). (n=3). (**F**) The intracellular location of berberine and mitochondria in MM-NPs was determined by confocal laser scanning microscopy (CLSM) imaging. Mito-red was used to mark intracellular mitochondria. Scale bar, 10 μm. (**G**) Plot profile for co-localization analysis of berberine and mitochondria in MM-NPs. (**H**) qPCR of the indicated cytokines in MLE-12 cells. (n=3). Data are from three experiments and presented as means ± SE. *P < 0.05, **P < 0.01, ***P < 0.001, ****P < 0.0001.

 https://doi.org/10.2147/IJN.S514611

responsive delivery nanoparticles and mitochondria, which is conducive to the occurrence of its oxidative environment-responsive release.

To test whether MM-NPs are effective, we used LPS-stimulated MLE-12 cells to compare the effects of each group. The results showed that MM-NPs (Conc. of Berberine 16 μg/mL) significantly reduced the expression of IL-1α, IL-6 and TNF-α compared with other groups, and showed a more significant effect on the up-regulation of anti-inflammatory IL-10 (Figure 3H). This indicates that MM-NPs have a good effect in the treatment of inflammation.

In vivo Fluorescence Imaging of MM-NPs in LPS-Induced Pneumonia Mice

To verify the targeting of nanoparticles to the lungs, we combined DID with the lung epithelial cell membranes coated on the outer layers of MM-NPs and MMC-NPs for staining, and synthesized RBPSe-NPs by replacing berberine with DID. Then, the nano-drugs (according to an equal dose of DID, 2 mg/kg) were injected into the ALI mouse model formed by LPS[44] (4 mg/kg) stimulation through the tail vein. Using a small animal in vivo imaging system, we monitored the distribution of these nanoparticles in ALI mice. The DID loaded in the nanoparticles emits red fluorescence. As shown in Figure 4A, the fluorescence intensity in the lungs of the MM-NPs group and the MMC-NPs group is stronger than that of the RBPSe-NPs group. In addition, through semi-quantitative analysis of lung fluorescence (Figure 4B), statistical differences in fluorescent signals were observed at 6 hours, and the fluorescence intensity reached the strongest at 24 hours, and was mainly eliminated at 72 hours after injection. The fluorescence intensity in the lungs of the MM-NPs group and the MMC-NPs group is stronger than that of the RBPSe-NPs group, indicating that the nanoparticles coated with lung epithelial cell membranes have better targeting to the lungs and can increase the accumulation of nanoparticles in the lungs. This is of great significance for the treatment of lung diseases, can increase the concentration of drugs in the lungs and enhance the therapeutic effect.

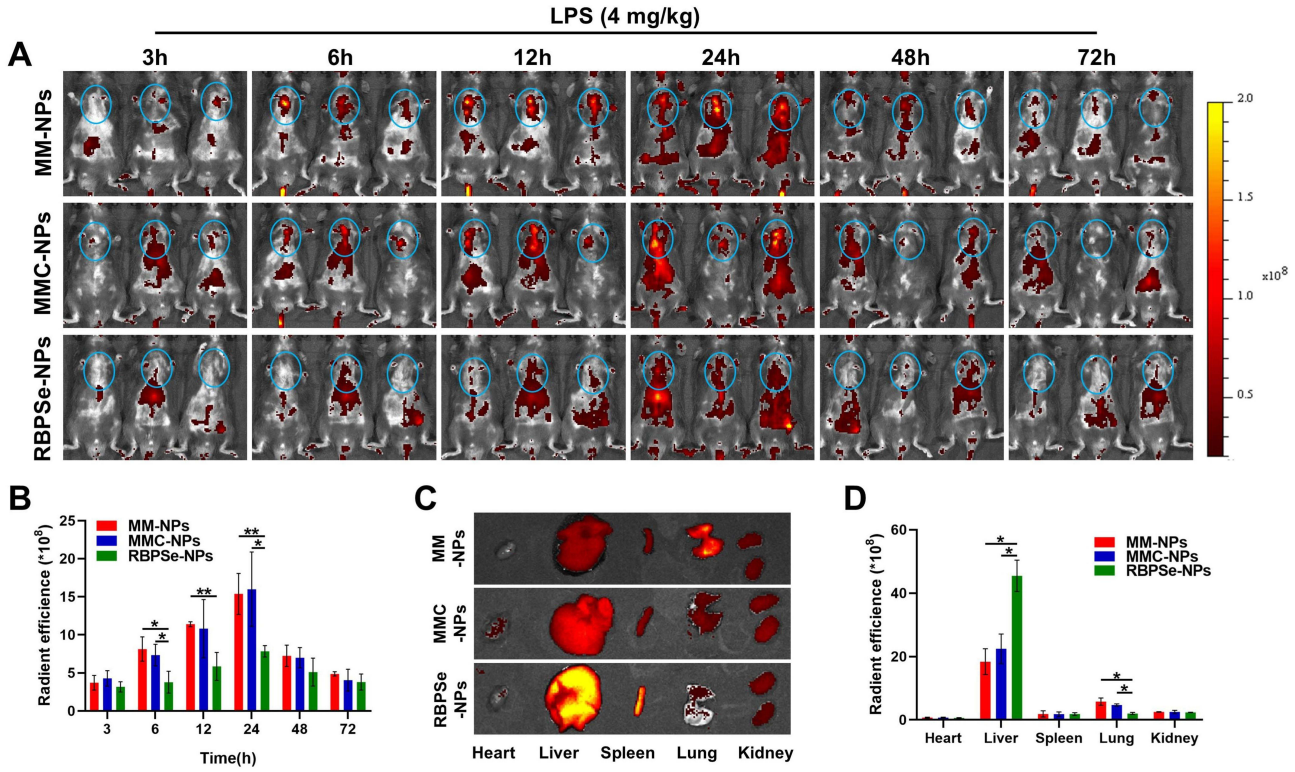

Figure 4 In vivo fluorescence imaging of MM-NPs in LPS-induced pneumonia mice. (**A**) Representative whole-body imaging of LPS-induced pneumonia mice at different time points after injection of MM-NPs, MMC-NPs and RBPSe-NPs. Combine DID with the outer cell membranes of MM-NPs and MMC-NPs for binding staining, and synthesize RBPSe-NPs by substituting DID for berberine. (DID, ex=535 nm, em=640 - 660 nm). (**B**) Quantitative analysis of the fluorescence imaging of mice from parallel images (**A**). (n=3). (**C**) Representative ex vivo imaging images of five major organs (heart, liver, spleen, lung and kidney) obtained from LPS-induced pneumonia mice at 72 hours after injection of MM-NPs, MMC-NPs and RBPSe-NPs. (**D**) Quantitative analysis of the fluorescence imaging of major organs from parallel images (**C**). (n=3). Data are presented as means ± SE. *P < 0.05, **P < 0.01.

https://doi.org/10.2147/IJN.S514611

After 72 hours of injecting nanoparticles, in the lungs of mice, it can still be seen that the fluorescence intensity of the MM-NPs group and the MMC-NPs group is stronger than that of the RBPSe-NPs group. However, the fluorescence at the liver shows the opposite trend (Figure 4C and D). After 72 hours of injecting nanoparticles, the difference in lung fluorescence intensity further confirms the effectiveness of lung epithelial cell membrane coating for lung targeting. The fluorescence intensity of MM-NPs/MMC-NPs in the liver is lower than that of RBPSe-NPs, suggesting that the membrane coating may reduce liver metabolism and lower the risk of non-target distribution throughout the body. At the same time, the relatively strong fluorescence in the liver compared to other organs indicates that a large amount of nano-drugs are metabolized through the liver.

Administration of MM-NPs Alleviates Lipopolysaccharide-Induced Lung Injury in Mice

To test that MM-NPs have a regulatory role in pulmonary immunopathology. We established a mouse model of acute lung injury[44] (ALI) by intratracheal instillation of endotoxin and administered MM-NPs to evaluate its effect (Figure 5A). After administering MM-NPs to endotoxin-stimulated mice, the total cell and protein counts leaked in bronchoalveolar lavage fluid (BALF) decreased (Figure 5B and C). It indicates that MM-NPs can reduce the inflammatory response caused by lung injury, reduce the leakage of cells and proteins, and have a certain protective effect on lung tissue. As expected, histological examination showed that endotoxin-stimulated mice showed increased thickening of the alveolar wall and increased cell infiltration. The treatment of MM-NPs significantly reduced inflammatory cell infiltration compared to other groups (Figure 5D). This further confirms the regulatory role of MM-NPs in pulmonary immunopathology. Reducing inflammatory cell infiltration can reduce inflammatory damage to lung tissue and promote the repair and regeneration of lung tissue.

As we all know, lung macrophages are heterogeneous, and different subsets have different phenotypes and functions.[45] Specifically, resident alveolar macrophages (AMs) in the lungs are crucial for pathogen clearance and tissue repair, while monocyte-derived macrophages (MMs) make important contributions to pulmonary immunopathology.[46–48] Our data shows that intratracheal instillation of endotoxin leads to an increase in the proportion of CD45+F4/80+CD11b+ MMs and CD45+Ly6G+CD11b+ neutrophils. These two major pro-inflammatory cell subsets are the basis for acute lung injury. Strikingly, the administration of MM-NPs reversed this trend and significantly reduced the infiltration of MMs and neutrophils in the lungs compared to other groups (Figure 5E and F). This indicates that MM-NPs have a regulatory role in pulmonary immunopathology and can inhibit the aggregation of pro-inflammatory cell subsets and reduce lung inflammation.

In addition, compared with other groups, the administration of MM-NPs significantly reduced the expression of IL-1α, IL-6 and TNF-α, and showed a more significant effect on the up-regulation of anti-inflammatory IL-10 (Figure 5G). In conclusion, the results indicate that MM-NPs treatment significantly reduces lung inflammation and improves lung pathology in mice under endotoxin attack, and increases the therapeutic effect of berberine on endotoxin-induced ALI.

In the above results study, we also compared the intervention effects of different ALI treatment groups: the PBS control group, the free berberine treatment group, the ROS-responsive berberine nano-micelle group (RBPSe-NPs), and the membrane-mimicking berberine nano-micelle group (MM-NPs). The PBS control group, as the control for the ALI model, did not show any therapeutic effect. The total cell count, protein leakage in BALF, and the levels of pro-inflammatory factors all increased significantly. The pathological damage of lung tissue (thickening of the alveolar wall and inflammatory cell infiltration) was the most severe, which verified the successful establishment of the ALI model and the disease progression without intervention. The free berberine treatment group only partially alleviated the cell leakage and pro-inflammatory factor levels in BALF, and had limited inhibitory effect on the inflammatory infiltration of lung tissue. This indicates that the traditional drug administration method is difficult to maintain an effective drug concentration in the lung lesions. The therapeutic effect of the RBPSe-NPs group was still significantly weaker than that of the MM-NPs. The possible reason is the lack of lung targeting ability. They are easily cleared by the mononuclear phagocyte system in the circulation, resulting in insufficient enrichment efficiency in lung tissue. Even if ROS triggers drug release, the local drug concentration at the lesion site is still limited. Although the MM-NPs are coated with lung epithelial cell

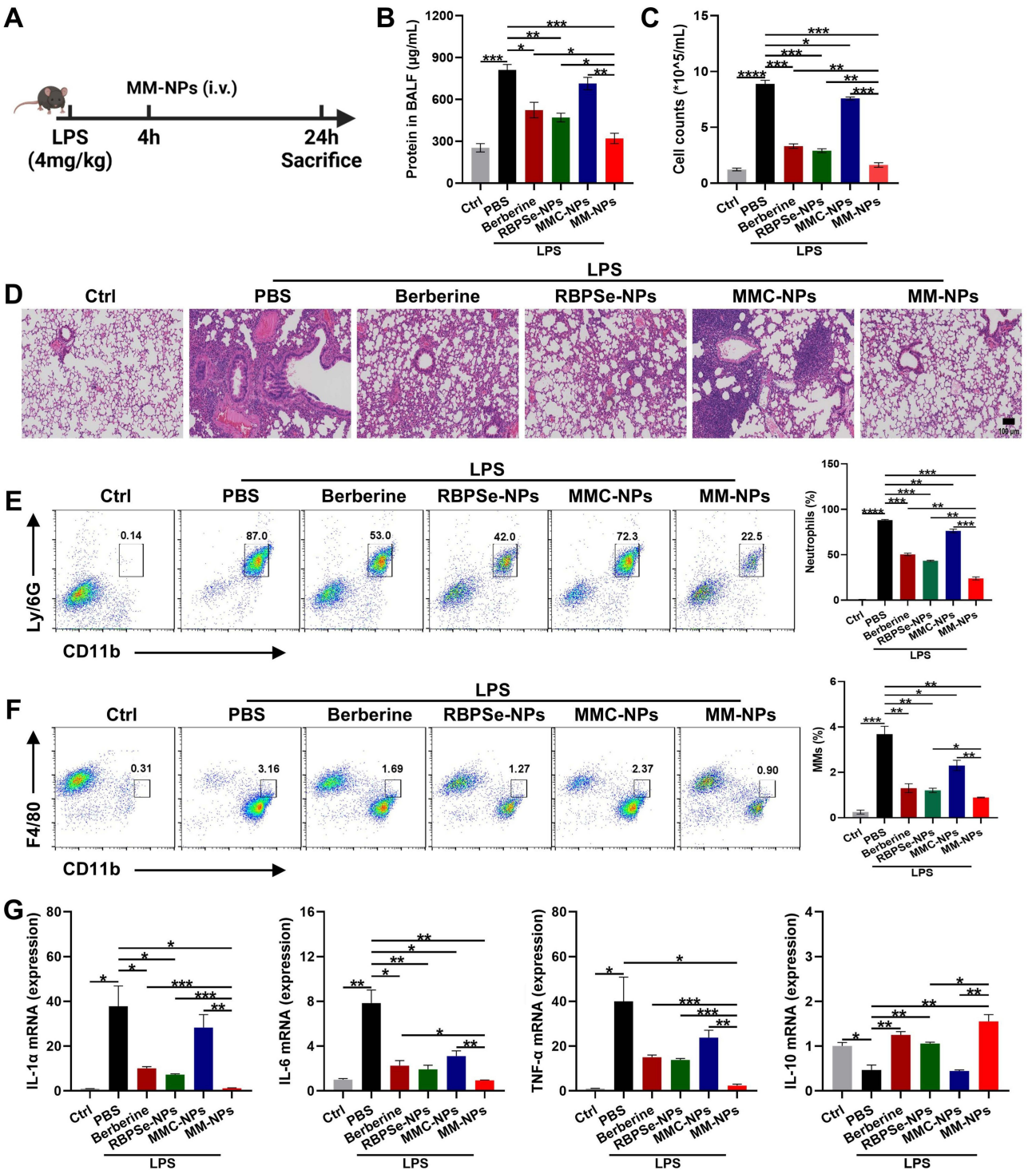

Figure 5 Administration of MM-NPs alleviates lipopolysaccharide-induced lung injury in mice. (**A**) Simplified experimental protocol. C57BL/6 mice (n=5) were intratracheally administered LPS (4 mg/kg) for 4 hours and then treated with MM-NPs (2 mg/kg of berberine, intravenously), etc. The mice were sacrificed after 24 hours. (**B**) Protein concentration in BALF. (n=3). (**C**) Total cell counts in BALF. (n=3). (**D**) H&E staining of lung tissues. Scale bar, 100 μm. (**E**) Flow cytometry of the ratios of CD45+CD11b+Ly6G+ neutrophils in BALF. (n=3). (**F**) Flow cytometry of the ratios of CD45+CD11b+F4/80+ MMs in BALF. (n=3). (**G**) qPCR of the indicated cytokines in lungs. (n=3). Data are presented as means ± SE. *P < 0.05, **P < 0.01, ***P < 0.001, ****P < 0.0001.

https://doi.org/10.2147/IJN.S514611

membranes, endowing the nanoparticles with homologous targeting ability, the lack of a ROS-responsive release mechanism makes drug release rely on passive diffusion or enzymatic hydrolysis processes. The release rate does not match the pathological needs of the lesion site. Its therapeutic effect was even weaker than that of the free berberine group, suggesting that simple targeted delivery cannot overcome the spatio-temporal limitations of drug release. Instead, it may weaken the therapeutic effect due to premature release or insufficient release. In conclusion, MM-NPs break through the bottleneck of single-functional nano-systems through the dual strategies of membrane-mimicking targeting and ROS-responsive release.

Mechanism Analysis of MM-NPs in the Treatment of Lipopolysaccharide-Induced Lung Injury Mice

To explore the potential mechanism of MM-NPs in the treatment of acute pneumonia, we analyzed the results of transcriptome sequencing (RNA-seq) of lung tissues from treated or untreated mice with acute lung injury. First, GSEA analysis showed that MM-NPs down-regulated the gene levels elevated by LPS stimulation and down-regulated the levels of inflammation-related genes (Figure 6A and B). This verifies the therapeutic effect of MM-NPs on acute pneumonia and alleviates the inflammatory response caused by LPS.

To further clarify the effects of MM-NPs on lung function and genetic pathways, we performed Kyoto Encyclopedia of Genes and Genomes (KEGG) and Gene Ontology (GO) analyses (Figure 6C and D). It was found that the functional differences between the control group and the treatment group were mainly concentrated on the "Signal transduction" and "cell part" pathways. This provides a direction for further research on the mechanism of action of MM-NPs. Immediately afterwards, volcano plot analysis showed (Figure 6E) that there were 471 differentially expressed genes with statistical significance, including 82 up-regulated genes (red) and 389 down-regulated genes (blue). Among the down-regulated genes, CCR5 (C-C chemokine receptor type 5), APOL6 (apolipoprotein L6), and NOXO1 (NADPH oxidase organizer 1) had the most significant statistical differences (Figure 6F). The gene CCR5 plays a regulatory role in the inflammatory response,[49] which suggests that MM-NPs may have a regulatory effect on the inflammatory response. The gene NOXO1 is involved in the oxidative stress response,[50] indicating that MM-NPs may also have a regulatory effect on oxidative stress. And the gene APOL6 may be related to inflammation or oxidative stress. In summary, MM-NPs may treat pneumonia by regulating inflammation and oxidative stress. The following analysis also verifies this statement. RNA sequencing found that MM-NPs attenuated the expression of a series of inflammatory cytokine, chemokine-related genes and oxidative stress-related genes in mice with acute pneumonia (Figure 6G and H).

The Safety of MM-NPs in vivo

MM-NPs have shown promise in treating ALI. We further evaluated the potential toxic effects caused by MM-NPs. In fact, H&E staining of tissue sections showed that nanoparticles did not induce significant tissue damage in the major organs of the heart, liver, spleen and kidney (Figure 7A). This indicates that MM-NPs do not cause obvious structural lesions in these important organs, suggesting good histocompatibility. Complete blood count shows that in mice receiving nano-therapy, the counts of platelets (PLT), red blood cells (RBC) and white blood cells (WBC) and the level of hemoglobin (HGB) did not change significantly (Figure 7B–E). This shows that MM-NPs have no significant adverse effects on the blood system and will not cause abnormal changes in blood components. In addition, nanoparticle treatment had no significant effect on the levels of alanine aminotransferase (ALT) and aspartate aminotransferase (AST), typical biomarkers of liver function, and the concentration of creatinine (CR), an indicator of renal function (Figure 7F–H). This further confirms that MM-NPs have no obvious damage to the functions of important organs such as the liver and kidney and have good biocompatibility. The data show that MM-NPs and related nanomaterials exhibit good biocompatibility and no obvious tissue toxicity. This provides an important safety basis for its further research and clinical application.

Regarding the long-term toxicity study of ROS-responsive materials with diselenide bonds in mice, some studies have mentioned that the degradation of diselenide bonds may produce selenoic acids, but no relevant toxicity was observed in

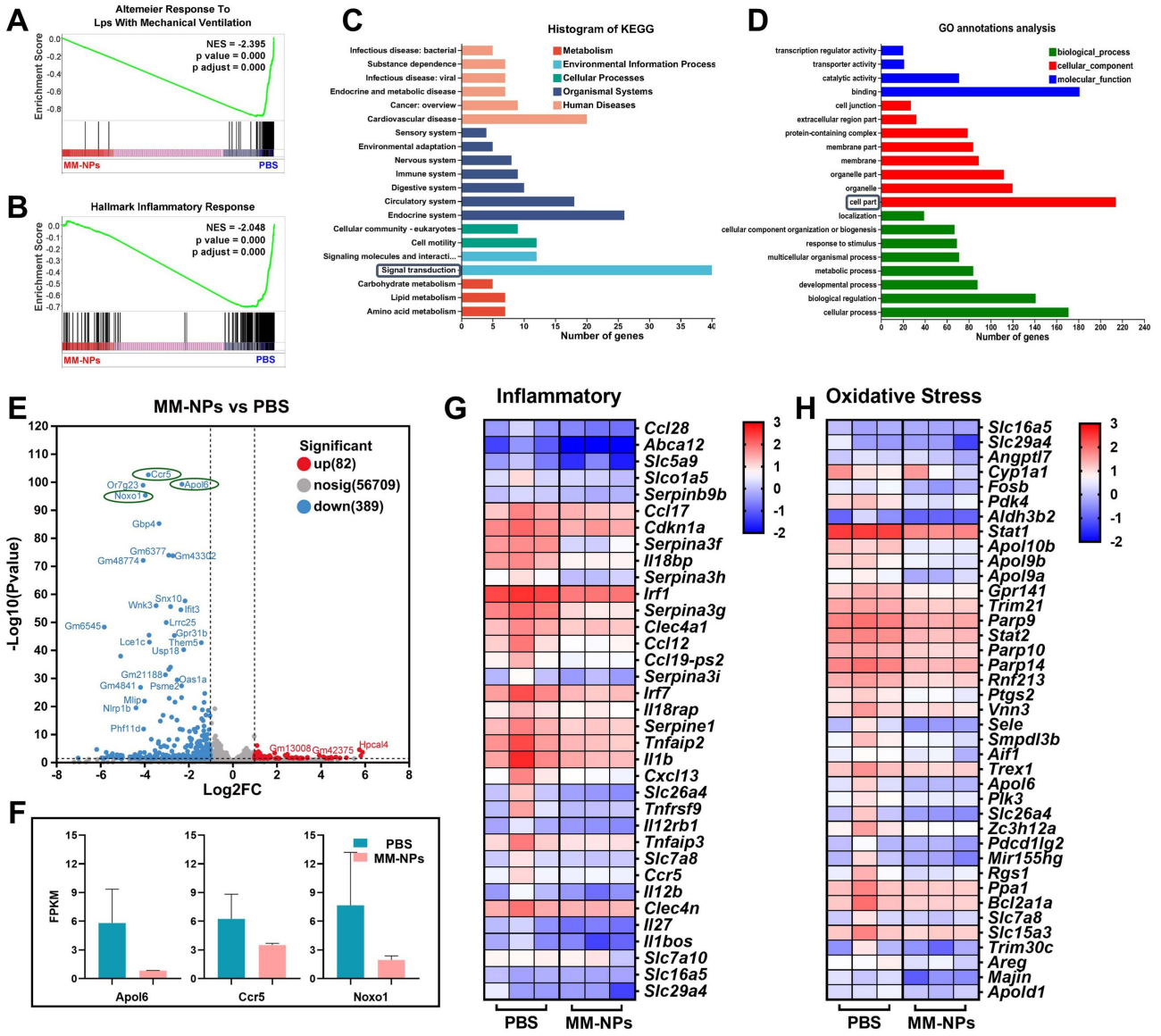

Figure 6 Transcriptome sequencing analysis of lipopolysaccharide-induced lung injury mice treated with MM-NPs. (**A**) GSEA results of the statistically significant gene set: Altemeier Response To Lps With Mechanical Ventilation. (**B**) GSEA results of the statistically significant gene set: Hallmark Inflammatory Response. (**C**) KEGG analysis of DEGs. (**D**) GO analysis of DEGs. (**E**) Volcano plot analysis of DEGs between PBS control or MM-NPs treated. (**F**) Fragments Per Kilobase of exon model per Million mapped fragments (FPKM) of some important genes. (**G**) Heat map of expression of inflammatory genes of PBS control or MM-NPs treated. (**H**) Heat map of expression of oxidative stress genes of PBS control or MM-NPs treated.

long-term mouse experiments.[51] Research on X-ray-responsive materials crosslinked by diselenide bonds also indicates their long-term safety.[52] Regarding the long-term toxicity study of PLGA and PEG used in the materials in mice, existing research shows that these two materials exhibit good biocompatibility in drug delivery systems. As a biodegradable material approved by the FDA, the degradation products of PLGA (lactic acid and glycolic acid) can be cleared through metabolic pathways. In the study, PLGA-PEG implants demonstrated the ability to release drugs continuously for 3 months in a mouse model, and no significant long-term toxicity was reported.[53] From the above studies, the safety of long-term application of the materials can be judged.

https://doi.org/10.2147/IJN.S514611

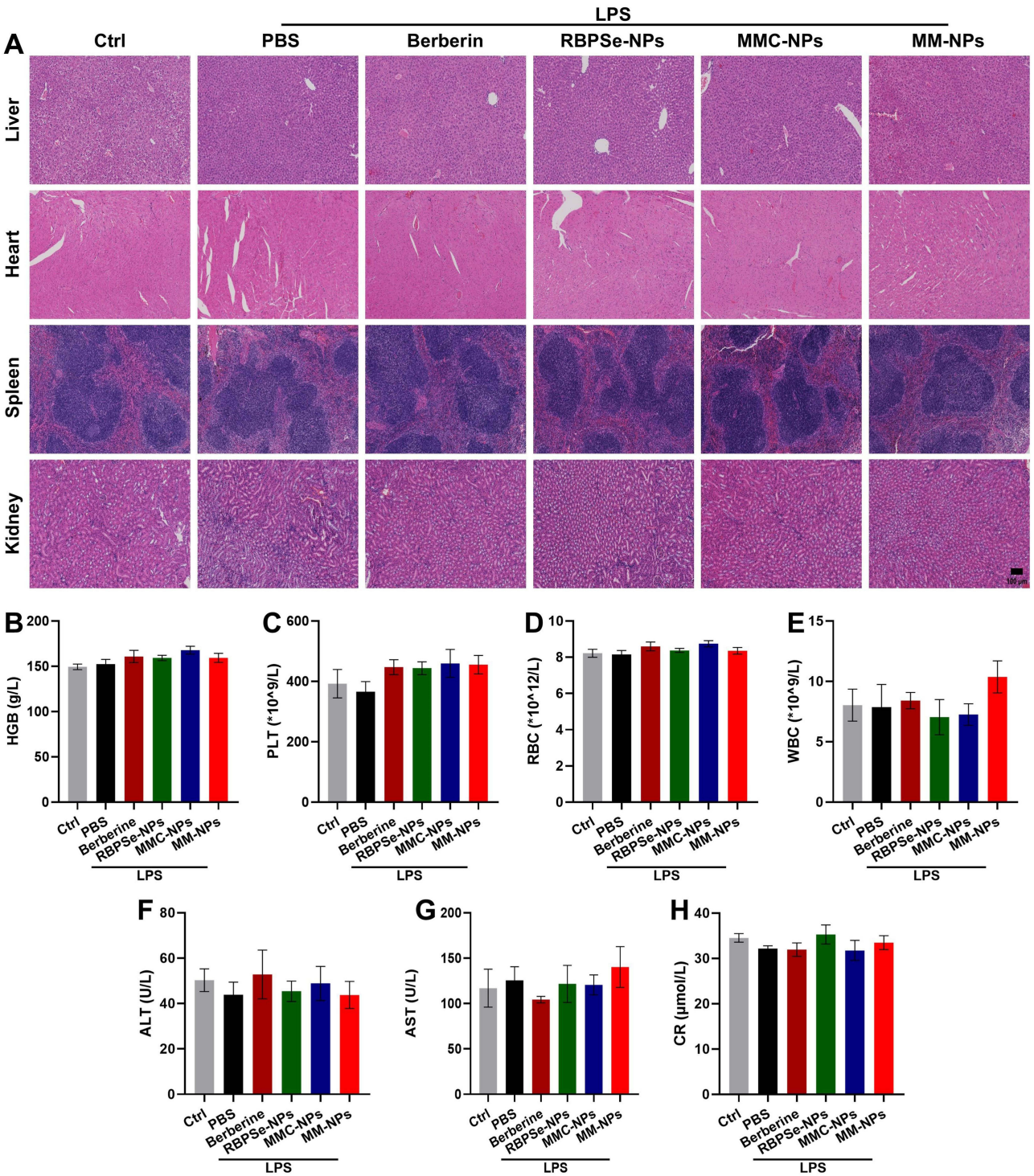

Figure 7 The safety of MM-NPs in vivo. (**A**) H&E staining of heart, liver, spleen and kidney tissues from the mice in different groups. Scale bar, 100 μm. (**B**) The levels of Hemoglobin (HGB). (**C**) The numbers of platelets (PLT). (**D**) The numbers of red blood cells (RBC). (**E**) The numbers of white blood cells (WBC). (**F**) The levels of alanine transaminase (ALT). (**G**) The levels of aspartate transaminase (AST). (**H**) The levels of creatinine (CR). (**B**–**H**, n=5). Data are presented as means ± SE.

Conclusion

We conducted in-depth research focusing on acute lung injury, which seriously threatens human health. We found that berberine can effectively alleviate pulmonary inflammation and promote lung tissue repair by inhibiting the release of inflammatory factors and reducing oxidative stress.

To improve the bioavailability of berberine, we constructed a novel delivery system, MM-NPs. This system uses ROS-responsive micelles to load berberine and is coated with lung epithelial cell membranes. It remains stable under normal physiological conditions. After entering the inflammatory area of acute lung injury, the diselenide bond breaks due to the increased ROS level, enabling precise drug release. The lung epithelial cell membrane enhances lung targeting. The surface proteins and receptors on it help the drug accurately reach the lesion site, reducing side effects on other organs and improving the safety and specificity of treatment.

In vitro studies have shown that MM-NPs have excellent physicochemical properties and good biocompatibility, in terms of stability, the micelles can remain stable for two weeks at 37 °C. The encapsulation efficiency of berberine in the micelles reaches 68.2%. The camouflage of lung epithelial cell membranes and the dynamic response of diselenide bonds enhance the lung-targeted accumulation of berberine, avoiding the risk of systemic toxicity caused by the enterohepatic circulation of free berberine and improving metabolic safety. Animal experiments further confirmed its effectiveness. MM-NPs can significantly improve the therapeutic effect of berberine on acute lung injury, improve the pathological state of the lungs, and promote the repair and regeneration of lung tissue. The current clinical intervention measures for acute lung injury, such as glucocorticoids, anti-inflammatory drugs, mechanical ventilation, and antibiotics, although each has its role, all have obvious limitations, including serious side effects, limited intervention effects, exacerbation of injury, or the development of drug resistance. Although no direct comparison has been made yet, from the existing data, MM-NPs show relative advantages in the treatment of acute lung injury. Their lung epithelial cell membrane biomimetic targeting can increase drug accumulation in the lungs and reduce systemic toxicity. The ROS-responsive release can achieve "treatment on demand", which is expected to bring new breakthroughs and hopes for the treatment of acute lung injury.

This study has successfully solved the problem of the bioavailability of berberine in the treatment of acute lung injury, providing a new and efficient solution for its treatment, opening up new ideas for research, and possessing important clinical application value and broad development prospects. Moreover, multiple studies have shown that ROS-responsive materials containing diselenide bonds, X-ray-responsive materials crosslinked by diselenide bonds, as well as PLGA and PEG used in the materials are safe for long-term application in mice.

In future research, in terms of clinical trials, multi-center trials and comparative trials can be carried out to provide sufficient evidence for clinical applications. Regarding alternative lung targeting strategies, explore new types of targeting carriers, gene editing-based strategies, and the combination of physical targeting technologies to expand the approaches for precise delivery.

Ethics Approval and Consent to Participate

Ethical approval Animal protocols were approved by the Scientific Investigation Committee of Zhejiang Laboratory Animal Center.

Consent for Publication

All authors of this study agreed to publish.

Funding

This study is supported in part by Construction of Traditional Chinese Medicine Inheritance and Innovation Development Demonstration Pilot Projects in Pudong New Area – High-Level Research-Oriented Traditional Chinese Medicine Hospital Construction (YC-2023-0901), Shanghai University of Traditional Chinese Medicine Science and Technology Development Fund (23KFL081), The fifth batch of "Longyi Scholar" Clinical Scientific and technological Innovation training Project of Longhua Hospital affiliated to Shanghai University of Traditional Chinese Medicine (PY2022011).

Disclosure

The authors declare that they have no known competing financial interests or personal relationships that could have appeared to influence the work reported in this paper.

References

1. Xia L, Zhang C, Lv N. et al. AdMSC-derived exosomes alleviate acute lung injury via transferring mitochondrial component to improve homeostasis of alveolar macrophages. *Theranostics*. 2022;12(6):2928–2947. doi:10.7150/thno.69533
2. Sapoznikov A, Gal Y, Falach R, et al. Early disruption of the alveolar-capillary barrier in a ricin-induced ARDS mouse model: neutrophil-dependent and -independent impairment of junction proteins. *Am J Physiol Lung Cell Mol Physiol*. 2019;316(1):L255–L268. doi:10.1152/ajplung.00300.2018
3. Ye L, Gao Y, Mok SWF, et al. Modulation of alveolar macrophage and mitochondrial fitness by medicinal plant-derived nanovesicles to mitigate acute lung injury and viral pneumonia. *J Nanobiotechnol*. 2024;22(1). doi:10.1186/s12951-024-02473-w
4. Guo Y, Liu Y, Zhao S, et al. Oxidative stress-induced FABP5 S-glutathionylation protects against acute lung injury by suppressing inflammation in macrophages. *Nat Commun*. 2021;12(1). doi:10.1038/s41467-021-27428-9
5. Meyer NJ, Gattinoni L, Calfee CS. Acute respiratory distress syndrome. *Lancet*. 2021;398(10300):622–637. doi:10.1016/s0140-6736(21)00439-6
6. Bellani G, Laffey JG, Pham T, et al. Epidemiology, patterns of care, and mortality for patients with acute respiratory distress syndrome in intensive care units in 50 countries. *JAMA*. 2016;315(8):788. doi:10.1001/jama.2016.0291
7. Pham T, Rubenfeld GD. Fifty years of research in ARDS. The epidemiology of acute respiratory distress syndrome. A 50th birthday review. *Am J Respir Crit Care Med*. 2017;195(7):860–870. doi:10.1164/rccm.201609-1773CP
8. Hayes M, Curley G, Ansari B, Laffey JG. Clinical review: stem cell therapies for acute lung injury/acute respiratory distress syndrome - hope or hype? *Critical Care*. 2012;16(2):205. doi:10.1186/cc10570
9. Levitt JE, Calfee CS, Goldstein BA, Vojnik R, Matthay MA. Early Acute Lung Injury. *Crit Care Med*. 2013;41(8):1929–1937. doi:10.1097/CCM.0b013e31828a3d99
10. Hassoun A, Linden PK, Friedman B. Incidence, prevalence, and management of MRSA bacteremia across patient populations—a review of recent developments in MRSA management and treatment. *Critical Care*. 2017;21(1). doi:10.1186/s13054-017-1801-3
11. Imenshahidi M, Hosseinzadeh H. Berberis Vulgaris and Berberine: an Update Review. *Phytother Res*. 2016;30(11):1745–1764. doi:10.1002/ptr.5693
12. Wang K, Yin J, Chen J, et al. Inhibition of inflammation by berberine: molecular mechanism and network pharmacology analysis. *Phytomedicine*. 2024;128:155258. doi:10.1016/j.phymed.2023.155258
13. Zhang S, Xu P, Zhu Z, et al. Acetylation of p65Lys310 by p300 in macrophages mediates anti-inflammatory property of berberine. *Redox Biol*. 2023;62:102704. doi:10.1016/j.redox.2023.102704
14. Chen L, Liu X, Wang X, Lu Z, Ye Y. Berberine alleviates acute lung injury in septic mice by modulating Treg/Th17 homeostasis and downregulating NF-κB signaling. *Drug Des Devel Ther*. 2023;17:1139–1151. doi:10.2147/dddt.S401293
15. White A, Wang Z, Wang X, et al. NLRP3 inflammasome activation in cigarette smoke priming for Pseudomonas aeruginosa-induced acute lung injury. *Redox Biol*. 2022;57:102467. doi:10.1016/j.redox.2022.102467
16. Wu YH, Wei CY, Hong WC, Pang JS. Berberine suppresses leukocyte adherence by downregulating CX3CL1 expression and shedding and ADAM10 in lipopolysaccharide-stimulated vascular endothelial cells. *Int J Mol Sci*. 2022;23. doi:10.3390/ijms23094801.
17. Khoshandam A, Imenshahidi M, Hosseinzadeh H. Pharmacokinetic of berberine, the main constituent of Berberis vulgaris L.: a comprehensive review. *Phytotherap Res*. 2022;36(11):4063–4079. doi:10.1002/ptr.7589
18. Yu Q, Li M, Chen H, et al. The discovery of berberine erythrocyte-hemoglobin self-assembly delivery system: a neglected carrier underlying its pharmacokinetics. *Drug Delivery*. 2022;29(1):856–870. doi:10.1080/10717544.2022.2036870
19. Su F, Zhang C, Zhang Q, et al. Multifaceted immunomodulatory nanocomplexes target neutrophilic-ROS inflammation in acute lung injury. *Adv Sci*. 2025;12(8):e2411823. doi:10.1002/advs.202411823
20. Bian Y, Li Y, Xia D, et al. Ionizable lipid nanoparticles enhance lung delivery of gold nanoclusters for improving acute lung injury alleviation. *Nanoscale*. 2025;17(13):7888–7897. doi:10.1039/d4nr05415f
21. Salido S, Alejo-Armijo A, Parola AJ, et al. Chitosan derivatives as nanocarriers for hLDHA inhibitors delivery to hepatic cells: a selective strategy for targeting primary hyperoxaluria diseases. *Int J Pharm*. 2022;627:122224. doi:10.1016/j.ijpharm.2022.122224
22. Aschmann D, Knol RA, Kros A. Lipid-based nanoparticle functionalization with coiled-coil peptides for in vitro and in vivo drug delivery. *Acc Chem Res*. 2024;57(8):1098–1110. doi:10.1021/acs.accounts.3c00769
23. Lins A, Keuter L, Mulac D, Humpf HU, Langer K. Are stabilizers, located on the surface of PLGA nanoparticles, able to modify the protein adsorption pattern? *Int J Pharm*. 2025;674:125488. doi:10.1016/j.ijpharm.2025.125488
24. Zou S, Wang B, Wang C, Wang Q, Zhang L. Cell membrane-coated nanoparticles: research advances. *Nanomedicine*. 2020;15(6):625–641. doi:10.2217/nnm-2019-0388
25. Yang X, Chen M, Weng C, et al. Red blood cell membrane-coated nanoparticles enable incompatible blood transfusions. *Adv Sci*. 2024;11. doi:10.1002/advs.202310230
26. Wang D, Wang S, Zhou Z, et al. White blood cell membrane-coated nanoparticles: recent development and medical applications. *Adv Healthcare Mater*. 2021;11. doi:10.1002/adhm.202101349
27. Zhuang J, Gong H, Zhou J, et al. Targeted gene silencing in vivo by platelet membrane–coated metal-organic framework nanoparticles. *Sci Adv*. 2020;6(13). doi:10.1126/sciadv.aaz6108
28. Zamora ME, Essien E-O, Bhamidipati K, et al. Marginated neutrophils in the lungs effectively compete for nanoparticles targeted to the endothelium, serving as a part of the reticuloendothelial system. *ACS Nano*. 2024;18(33):22275–22297. doi:10.1021/acsnano.4c06286
29. Belyaev IB, Griaznova OY, Yaremenko AV, Deyev SM, Zelepukin IV. Beyond the EPR effect: intravital microscopy analysis of nanoparticle drug delivery to tumors. *Adv Drug Delivery Rev*. 2025;219:115550. doi:10.1016/j.addr.2025.115550
30. Zhao H, Li L, Peng Z, et al. Improved targeting delivery of WED-load immunoliposomes modified with SP-A mAb for the treatment of pulmonary fibrosis. *Colloids Surf B*. 2023;224:113237. doi:10.1016/j.colsurfb.2023.113237
31. Staquicini DI, Cardó-Vila M, Rotolo JA, et al. Ceramide as an endothelial cell surface receptor and a lung-specific lipid vascular target for circulating ligands. *Proc Natl Acad Sci USA*. 2023;120:e2220269120, doi:10.1073/pnas.2220269120
32. Jafari H, Mahdavinia GR, Kazemi B, et al. Highly efficient sunitinib release from pH-responsive mHPMC@Chitosan core-shell nanoparticles. *Carbohydr Polym*. 2021;258:117719. doi:10.1016/j.carbpol.2021.117719

33. Brion A, Chaud J, Léonard J, et al. Red light-responsive upconverting nanoparticles for quantitative and controlled release of a coumarin-based prodrug. *Adv Healthcare Mater*. 2022;12(2). doi:10.1002/adhm.202201474
34. Zhang H, Xu X, Shou X, et al. Senolytic therapy enabled by senescent cell-sensitive biomimetic melanin nano-senolytics. *Adv Healthcare Mater*. 2024. doi:10.1002/adhm.202401085
35. Yadav S, Ramesh K, Reddy OS, et al. Redox-responsive comparison of diselenide and disulfide core-cross-linked micelles for drug delivery application. *Pharmaceutics*. 2023;15(4):1159. doi:10.3390/pharmaceutics15041159
36. Shi Z, Liu J, Tian L, et al. Insights into stimuli-responsive diselenide bonds utilized in drug delivery systems for cancer therapy. *Biomed Pharmacothe*. 2022;155:113707. doi:10.1016/j.biopha.2022.113707
37. Kondengadan SM, Wang B. Quantitative factors introduced in the feasibility analysis of reactive oxygen species (ROS)-sensitive triggers. *Angew Chem*. 2024;63(26):e202403880. doi:10.1002/anie.202403880
38. Fan X-X, Xu M-Z, Leung EL-H, et al. ROS-responsive berberine polymeric micelles effectively suppressed the inflammation of rheumatoid arthritis by targeting mitochondria. *Nano-Micro Lett*. 2020;12(1). doi:10.1007/s40820-020-0410-x
39. Ma N, Li Y, Xu H, Wang Z, Zhang X. Dual redox responsive assemblies formed from diselenide block copolymers. *J Am Chem Soc*. 2009;132 (2):442–443. doi:10.1021/ja908124g
40. Deepagan VG, Kwon S, You DG, et al. In situ diselenide-crosslinked polymeric micelles for ROS-mediated anticancer drug delivery. *Biomaterials*. 2016;103:56–66. doi:10.1016/j.biomaterials.2016.06.044
41. Cen M, Ouyang W, Zhang W, et al. MitoQ protects against hyperpermeability of endothelium barrier in acute lung injury via a Nrf2-dependent mechanism. *Redox Biol*. 2021;41:101936. doi:10.1016/j.redox.2021.101936
42. Shou X, Chen C, Ying H, et al. Biomimetic MOF nanocarrier-mediated synergistic delivery of mitochondria and anti-inflammatory miRNA to alleviate acute lung injury. *Adv Sci*. 2025;12(16):e2416594. doi:10.1002/advs.202416594
43. Dolcet X, Llobet D, Pallares J, Matias-Guiu X. NF-kB in development and progression of human cancer. *Virchows Archiv*. 2005;446(5):475–482. doi:10.1007/s00428-005-1264-9
44. Yu W-W, Lu Z, Zhang H, et al. Anti-inflammatory and protective properties of Daphnetin in endotoxin-induced lung injury. *J Agri Food Chem*. 2014;62(51):12315–12325. doi:10.1021/jf503667v
45. Aegerter H, Lambrecht BN, Jakubzick CV. Biology of lung macrophages in health and disease. *Immunity*. 2022;55(9):1564–1580. doi:10.1016/j.immuni.2022.08.010
46. Malainou C, Abdin SM, Lachmann N, Matt U, Herold S. Alveolar macrophages in tissue homeostasis, inflammation, and infection: evolving concepts of therapeutic targeting. *J Clin Investig*. 2023;133(19). doi:10.1172/jci170501
47. Min B, Grant-Orser A, Johannson KA. Peripheral blood monocyte count and outcomes in patients with interstitial lung disease: a systematic review and meta-analysis. *Eur Respir Rev*. 2023;32(169):230072. doi:10.1183/16000617.0072-2023
48. Neupane AS, Willson M, Chojnacki AK, et al. Patrolling alveolar macrophages conceal bacteria from the immune system to maintain homeostasis. *Cell*. 2020;183(1):110–125.e111. doi:10.1016/j.cell.2020.08.020
49. Lin Y, Liu S, Sun Y, et al. CCR5 and inflammatory storm. *Ageing Res Rev*. 2024;96:102286. doi:10.1016/j.arr.2024.102286
50. Buchmann GK, Schürmann C, Warwick T, et al. Deletion of NoxO1 limits atherosclerosis development in female mice. *Redox Biol*. 2020;37:101713. doi:10.1016/j.redox.2020.101713
51. Lessa T, Correia TML, Santos TCD, et al. A novel diselenide attenuates the carrageenan-induced inflammation by reducing neutrophil infiltration and the resulting tissue damage in mice. *Free Radical Res*. 2024;58(4):229–248. doi:10.1080/10715762.2024.2336566
52. Chen R, Gong J, Yu Z, et al. X-ray triggered bimetallic nanoassemblies as radiosensitizers and STING agonists for a CDT/radio-immunotherapy strategy. *Acta Biomater*. 2025;192:366–376. doi:10.1016/j.actbio.2024.12.030
53. Lehner E, Honeder C, Knolle W, et al. Towards the optimization of drug delivery to the cochlear apex: influence of polymer and drug selection in biodegradable intracochlear implants. *Int J Pharm*. 2023;643:123268. doi:10.1016/j.ijpharm.2023.123268